PHYSICAL REVIEW B **79**, 020404(R) (2009)

Incommensurate magnetic structure of YMn_2O_5: A stringent test of the multiferroic mechanism

P. G. Radaelli,[1,2] C. Vecchini,[1,3] L. C. Chapon,[1] P. J. Brown,[4] S. Park,[5] and S-W. Cheong[5]
[1]*ISIS Facility, Rutherford Appleton Laboratory, STFC, Chilton, Didcot, Oxfordshire OX11 0QX, United Kingdom*
[2]*Department of Physics and Astronomy, University College London, Gower Street, London WC1E 6BT, United Kingdom*
[3]*Institute of Electronic Structure and Laser, Foundation for Research and Technology–Hellas, Vassilika Vouton, 711 10 Heraklion, Crete, Greece*
[4]*Institut Laue-Langevin, 6 Rue Jules Horowitz, BP 156, 38042 Grenoble Cedex 9, France*
[5]*Department of Physics and Astronomy, Rutgers University, Piscataway, New Jersey 08854, USA*
(Received 12 November 2008; published 16 January 2009)

We have determined the magnetic structure of the low-temperature incommensurate phase of multiferroic YMn_2O_5 using single-crystal neutron diffraction. By employing corepresentation analysis, we have ensured full compliance with both symmetry and physical constraints, so that the electrical polarization must lie along the *b* axis, as observed. The evolution of the spin components and propagation through the commensurate-incommensurate phase boundary identifies the exchange-striction mechanism as the primary driving force for ferroelectricity.

DOI: 10.1103/PhysRevB.79.020404 PACS number(s): 75.25.+z, 28.20.Cz, 77.80.−e

The family of compounds with general formula RMn_2O_5 (R=Y, Bi, and La; rare earth) (Ref. 1) occupies a special place among the so-called novel multiferroic materials, in which ferroelectricity is directly induced by the onset of inversion-breaking magnetic ordering. In fact, whereas for most other multiferroics, such as $TbMnO_3$,[2,3] $Ni_3V_2O_8$,[4] and many other materials, the so-called spin-orbit (SO) mechanism[5,6] has clearly been identified as the primary driving force for the electrical polarization, the origin of ferroelectricity in RMn_2O_5 remains controversial. Three aspects of the RMn_2O_5 phenomenology suggest that the SO mechanism may not play a major role: the direction of the electrical polarization cannot be rotated by an applied magnetic field;[7] the main ferroelectric phase is magnetically *commensurate* while the low-temperature incommensurate phase (LTICP) is only weakly ferroelectric; and, most importantly, in the ferroelectric commensurate phase (CP), moments in the *ab* plane are almost collinear (noncollinearity is a strict requirement of the SO mechanism). An alternative explanation, based on the simple exchange-striction (ES) mechanism in the context of an acentric quasicollinear structure, has been shown to account qualitatively for the ferroelectric behavior of the different magnetic phases,[8,9] and recent electronic structure calculations not including the SO interaction[10] have reproduced the observed value of the electrical polarization P for certain values of the parameters. However, up to now the SO mechanism could not be completely ruled out, since accurate neutron-diffraction determinations of the CP magnetic structure[11,12] have identified a small cycloidal component in the ferroelectric phases.

One striking experimental fact about RMn_2O_5 is the sudden dramatic reduction in the value of P at the CP to LTICP transition. Understanding how the different components of the magnetic structure change could provide key insight into the multiferroic mechanism. More specifically, we have shown[13] that starting from the experimental magnetic structure, one can construct time-reversal-even polar vectors *specific* to each mechanism, which are directly proportional to the SO and ES contributions to P. Most likely, the coupling constants do not change across the transition; therefore, the magnitude of the electrically active polar vector *must*, like P, be greatly reduced across the transition. For this approach to be valid, the magnetic structures must be known with great accuracy. In this respect, YMn_2O_5 is an ideal system since there is no rare-earth magnetic ordering involved. At present, whereas the YMn_2O_5 CP magnetic structure is well established and has been validated independently by two groups,[11,12] the LTICP structure is not known with confidence. The two structures presented to date from neutron powder diffraction,[14] and more recently from single-crystal data,[15] are significantly different and, crucially, none of them exploits the full set of symmetry and physical constraints, requiring that the residual electrical polarization in the LTICP remains parallel to the *b* axis.

Here, we present a single-crystal neutron-diffraction determination of the YMn_2O_5 incommensurate magnetic structure that is fully compliant with symmetry and physical constraints. In particular, we have employed corepresentation analysis to impose the $\cdot 2 \cdot$ point-group symmetry, which is lower than the CP symmetry ($m2m$) but still guarantees that all the contributions to P are directed along the *b* axis, as observed experimentally. The fit to the data, collected on two independent magnetic domains, is much better than for previous structures[14,15] and is essentially equivalent to our best unconstrained refinement. The spins responsible for the ES polarization are now found to be nearly perpendicular and are modulated with opposite phases, leading to an ES polar vector smaller by a factor of 9 with respect to the CP. On the contrary, the magnitudes of the SO polar vectors *increase* significantly in the LTICP, while a new polar vector of SO origin and of smaller magnitude develops due to the formation of long-period cycloids along the *a* axis. Barring an accidental cancellation of SO terms, which is extremely unlikely to occur for all RMn_2O_5 compounds and all temperatures, this argues conclusively that ferroelectricity in the RMn_2O_5 commensurate phases is predominantly of exchange-strictive origin. However, it is possible that the SO mechanism may provide a contribution to the residual polarization in the low-temperature incommensurate phase.

The YMn_2O_5 single crystal for this study is the same as for Ref. 11 and the growth protocol is described therein. The experimental setup was also the same but the data were col-

TABLE I. Small irreps (Δ) and coreps (D) of space group *Pbam* for propagation vector $k_3=(\mu,0,\mu)$. The symmetry operators are in the Kovalev notation, $\epsilon=e^{-2\pi i k_x/2}=0.0628-i0.998$.

	h_1	h_{27}	Kh_{25}	Kh_3
Δ_1/D_1	1	ϵ	1	ϵ
Δ_2/D_2	1	$-\epsilon$	1	$-\epsilon$

lected at 2 K. The main difference between the experiments on the CP and LTICP phases is at the data reduction stage; in the CP with propagation vector $k=2\pi(\frac{1}{2},0,\frac{1}{4})$, there are two inversion-related domains that scatter onto the same points in reciprocal space, yielding single Bragg peaks on the position-sensitive detector (PSD). On the other hand, the LTICP has four distinct domains related by inversion and/or rotation around the c axis. The rotation-related domains have propagation vectors $k_1=2\pi(0.48,0,0.28)$ and $k_2=2\pi(-0.48,0,0.28)$. Scattering from these domains occurs at close positions in reciprocal space, yielding split peaks on the PSD. An *ad hoc* piece of software was developed to deconvolute the peaks from the two domains and exclude the reflections that were completely overlapped. Because of the different integration methods employed for the CP and LTICP, absolute scaling of the magnetic moments was verified using the neutron powder-diffraction data reported in Ref. 14. The FULLPROF program[16] was used for the refinements of the magnetic structure. In the final analysis, reflections from the two domains were combined in a single refinement, with the spin components of the two domains constrained by symmetry (see below).

For the *corep* analysis, we use the Kovalev conventions as in Ref. 17. The propagation vector is $k=2\pi(0.48,0,0.28)$ (k_3 in the Kovalev notation). The little *irrep* group contains two operators—the identity h_1 and the a-glide h_{27} perpendicular to b. According to Kovalev (see Table I), there are only two irreps, both one dimensional, each generating a corep. Both sites, Mn^{3+} and Mn^{4+}, split into two orbits in the little group, which are then recombined by the coreps. The transformation matrix β is the identity. The axial-vector modes were symmetrized with respect to the center of symmetry located at position 0,0.5,0.5. The twofold screw h_3 is located at $0.5,y,0.5$. In this respect we depart from Kovalev's conventions. Magnetic structures built from single-corep modes are by construction invariant by inversion (h_{25}) and are also invariant by rotation around the b axis (h_3) and reflection through a plane perpendicular to the b axis (h_{27}), except for the phase factor ϵ or $-\epsilon$, which, in an incommensurate structure, is always equivalent to a translation and does not affect the point-group symmetry. Our aim is to construct a magnetic structure that allows the development of polarization along the b axis—we want to drop the h_{25} and h_{27} invariance but retain the h_3 rotation around b (point-group symmetry $\cdot 2\cdot$). Inspection of Table I immediately suggests that this is accomplished by the combination D_1+iD_2. In fact, inversion and rotation appear in the little corep group as antiunitary operators. The imaginary unit in front of D_2 yields a sign change for these operators, ensuring the correct symmetry behavior.

As usual, each corep mode for a single spin component has two parameters—an amplitude and a phase, with the latter describing the phase difference between inversion-related sites. Therefore, the most generic magnetic structure invariant by $\cdot 2\cdot$ symmetry is described by 24 parameters (2 parameters $\times$ 3 spin components $\times$ 2 coreps $\times$ 2 sites). However, this number can be further reduced by imposing *physical* constraints. Sites related by inversion in the paramagnetic phase have almost identical magnetic environments (except for the tiny ferroelectric displacements). Hence, we expect not only that the wave amplitudes will be identical but also that the spins follow the same propagation except for a phase offset. This reduces the number of phases per site from 6 to 1 and the total number of parameters to 14. One of these parameters represents the overall phase and can also be fixed (we have chosen to fix $ub_x^2=0$) (see below), yielding 13 parameters in total, a drastic reduction from 48 for an unconstrained refinement.[15]

The j component of the magnetic moment on site l and unit cell n (at a position R_n from the origin) is written as

$$m_j^l(n) = S_j^l e^{ik\cdot R_n} + \text{c.c.} \tag{1}$$

The Fourier coefficients have been parametrized as, for example, for component x of site b,

$$S_x^b = \frac{1}{2}(ub_x^1 + iub_x^2)e^{i\Phi}, \tag{2}$$

where Φ is a global phase common to all components. The refined parameters for domain 1 and the appropriate transformation to obtain those of domain 2 are listed in Table II. The fit is far superior to that obtained using the model by Kim *et al.*[15] ($R_F \simeq 6.7\%$ vs 15.5% for Kim *et al.*) and is better than any unconstrained refinement we could obtain based on a simulated annealing structure. The magnetic structure of the LTICP is depicted in Fig. 1. The top panel shows the *ab*-plane projection of the *envelope* of the magnetic structure, i.e., several spin orientations describing a complete period of propagation are shown on the same site. The bottom panel shows a perspective view of the magnetic structure illustrating the phase relations between spins on different sites. The LTICP adopts the most generic type of single-k structure, in which spins rotate in an arbitrary plane with an elliptical envelope—in other words, all spin components are involved in the cycloids. These envelopes are strictly related by symmetry on the different Mn^{3+} and Mn^{4+} sites, and differ only by a phase factor. Mn^{3+} and Mn^{4+} envelopes are almost coplanar, but the Mn^{3+} ellipse is much more eccentric (the semiaxes are 3.65 and $2.21\mu_B$ for Mn^{3+}, and 2.48 and $2.00\mu_B$ for Mn^{4+}), reflecting the different anisotropy of the two sites. The Mn^{3+} long semiaxis coincides with the pyramid axis, consistent with the easy magnetic axis from susceptibility measurements and also with the results on the CP, whereas the short semiaxis points toward one of the oxygen atoms in the pyramid. The most important aspect of this structure is the *out-of-phase* relation between zig-zag chains running along the a axis (bottom panel of Fig. 1). This has two consequences: first, neighboring spins on different chains are essentially orthogonal; second, even when the angle is not

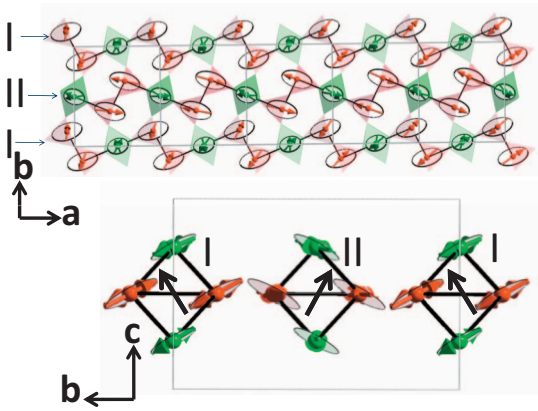

FIG. 1. (Color) Low-temperature incommensurate magnetic structure of YMn_2O_5. Top: projection of the magnetic structure onto the *ab* plane. Mn^{3+} and Mn^{4+} are shown with red and green colors, respectively. The ellipsoidal contours, more elongated for Mn^{3+}, show the envelope of the magnetic modulations. Adjacent antiferromagnetic zig-zag chains, labeled I and II, are shown by thick black lines. Bottom: projection of the magnetic structure onto the *bc* plane. The black arrows represent the normal direction to the ellipsoidal modulations in chains I and II.

90° due to the eccentricity, the dot product across chains cancels out almost exactly due to the sign change in different parts of the structure. As the ES polarization is proportional to this dot product, we argue that this loss of phase coherence is the primary cause of the loss of ferroelectricity in the LTICP (see below). As in many other cycloidal magnets, the CP to LTICP transition can be well explained in terms of competition between anisotropy (which favors quasicollinear arrangements) and entropy (which favors large-moment cycloids at low temperatures), but intriguingly, in RMn_2O_5 the ferroelectric properties of the two phases are *reversed* with respect to $TbMnO_3$.[2] In order to calculate the different contributions to the polarization, it is useful to extract modules (m_i) and phases (ϕ_i^u) for the complex arrays z_a and z_b defined as $z_{ax}=ua_x^1+iua_x^2$, etc.,

$$\phi_a^u = \arg(z_a), \quad \phi_b^u = \arg(z_b), \quad m_a = |z_a|, \quad m_b = |z_b|. \quad (3)$$

Using these equations, one can readily calculate all the macroscopic quantities of interest, and in particular the polar vectors corresponding to the different mechanisms.[13] Since the point-group symmetry is ·2·, only the *y* component of any polar vector will be nonzero. This can readily be verified by calculating the vector component explicitly, but it is not shown here. By employing the transformations in Table II, we can also verify explicitly that all the polar vectors change sign in domain 2. The formulas given here below are valid for the LTICP (no umklapp term[13]), while for the CP we use Eqs. (3) and (4) of Ref. 13. The ES polar vector is calculated as

$$E_y = \sum_{j=1}^{3} m_{aj} m_{bj} [4 \cos \psi_b \sin \psi_a \sin(\phi_{bj}^u - \phi_{aj}^u)]. \quad (4)$$

The two spin-orbit components that were already present in the CP, originating from *bc*-plane cycloids and relating to SO

TABLE II. YMn_2O_5 LTICP magnetic structure at $T=2$ K. Parametrized Fourier coefficients for domain 1, $k_1=2\pi(0.48,0,0.28)$. The refined values are $ub_x^1=-2.45(3)$, $ub_y^1=0.30(6)$, $ub_z^1=-0.27(10)$, $ub_x^2=0$, $ub_y^2=1.72(1)$, $ub_z^2=1.03(3)$, $\psi_b=-0.36(1)$, $ua_x^1=3.50(3)$, $ua_y^1=0.46(8)$, $ua_z^1=0.26(7)$, $ua_x^2=-0.53(8)$, $ua_y^2=-2.00(1)$, $ua_z^2=1.20(4)$, and $\psi_a=-1.650(7)$. $R_F=6.75/6.67\%$ and $R_F^2=10.7/9.83\%$ for domain 1 and domain 2, respectively. The transformations to obtain the domain 2 parameters are $k_2=2\pi(-0.48,0,0.28)$, $u_x^1\rightarrow -u_x^1$, $u_y^1\rightarrow -u_y^1$, $u_z^1\rightarrow u_z^1$, $u_x^2\rightarrow -u_x^2$, $u_y^2\rightarrow -u_y^2$, and $u_z^2\rightarrow u_z^2$ for both *a* and *b* sites, and $\psi_b\rightarrow\psi_b$ and $\psi_a\rightarrow -\psi_a$. Labeling of atoms is as in Ref. 11. Table IV in the appendix contains a complete list of parameters for both domains using the FULLPROF conventions.

Site	Fourier coefficients						Global phase Φ
b1	$+ub_x^1$	$+ub_y^1$	$+ub_z^1$	$+ub_x^2$	$+ub_y^2$	$+ub_z^2$	ψ_b
b2	$+ub_x^1$	$+ub_y^1$	$+ub_z^1$	$+ub_x^2$	$+ub_y^2$	$+ub_z^2$	$-\psi_b$
b3	$-ub_x^1$	$+ub_y^1$	$-ub_z^1$	$+ub_x^2$	$-ub_y^2$	$+ub_z^2$	$q_x/2+\psi_b$
b4	$-ub_x^1$	$+ub_y^1$	$-ub_z^1$	$+ub_x^2$	$-ub_y^2$	$+ub_z^2$	$q_x/2-\psi_b$
a1	$+ua_x^1$	$+ua_y^1$	$+ua_z^1$	$+ua_x^2$	$+ua_y^2$	$+ua_z^2$	ψ_a
a2	$-ua_x^1$	$+ua_y^1$	$-ua_z^1$	$+ua_x^2$	$-ua_y^2$	$+ua_z^2$	$q_x/2-\psi_a$
a3	$-ua_x^1$	$+ua_y^1$	$-ua_z^1$	$+ua_x^2$	$-ua_y^2$	$+ua_z^2$	$q_x/2+\psi_a$
a4	$+ua_x^1$	$+ua_y^1$	$+ua_z^1$	$+ua_x^2$	$+ua_y^2$	$+ua_z^2$	$q_x-\psi_a$

interactions across the Mn^{3+} planes (S_y^1) and *Y* planes (S_y^2), are

$$S_y^1 = m_{by} m_{bz} [-2 \sin 2\psi_b \sin(\phi_{by}^u - \phi_{bz}^u)],$$

$$S_y^2 = m_{by} m_{bz} [2 \sin(2\psi_b + q_z) \sin(\phi_{by}^u - \phi_{bz}^u)]. \quad (5)$$

In order to evaluate the spin-orbit contribution due to the in-plane projection of the cycloids (which was absent in the CP), we only consider the Mn^{3+}-Mn^{4+} within the chains, since the other bonds have a small projection on the direction of propagation (spins on Mn^{3+} atoms related by inversion are also almost antiparallel),

$$L_y = -4 \sin(q_x/2 - \psi_a) \cos \psi_b \cos \alpha [m_{bx} m_{ay} \sin(\phi_{bx}^u + \phi_{ay}^u) + m_{by} m_{ax} \sin(\phi_{by}^u + \phi_{ax}^u)]. \quad (6)$$

Table III lists the polar-vector components for the CP (Ref. 11) and LTICP, as determined from the previous formulas. The relative signs of the different components are uniquely established, but the overall sign depends on the choice of domain. Table III provides a stringent test for the multiferroic mechanisms; the drop of the ES component E_y is by far

TABLE III. Exchange-striction (E_y) and spin-orbit (S_y^1, S_y^2, and L_y) polar vectors for the CP and LTICP phases of YMn_2O_5. All the values are in μ_B^2. Statistical errors are propagated from the magnetic structure refinements.

Phase	E_y	S_y^1	S_y^2	L_y
CP	22.6(5)	−0.16(4)	−0.40(5)	0
LTICP	−2.5(3)	−1.01(8)	−1.3(1)	0.7(3)

TABLE IV. YMn_2O_5 LTICP magnetic structure at $T=2$ K for the two domains using the FULLPROF conventions. The FULLPROF code uses the *complex-conjugate* Fourier coefficient [Eq. (1)]. The FULLPROF parameters are therefore obtained from the one in Table II by changing all the signs of the imaginary components (the ones with the superscript 2). Global phases keep the same sign but are divided by 2π.

Name	M_x	M_y	M_z	iM_x	iM_y	iM_z	M_{phas}
				D_1			
b1	−2.45(3)	0.30(7)	−0.27(9)	0.000	−1.72(1)	−1.03(3)	−0.058(1)
b2	−2.45(3)	0.30(7)	−0.27(9)	0.000	−1.72(1)	−1.03(3)	0.058(1)
b3	2.45(3)	0.30(7)	0.27(9)	0.000	1.72(1)	−1.03(3)	0.183(1)
b4	2.45(3)	0.30(7)	0.27(9)	0.000	1.72(1)	−1.03(3)	0.298(1)
a1	3.50(3)	0.46(8)	0.26(7)	0.53(8)	2.00(1)	−1.20(4)	−0.263(1)
a2	−3.50(3)	0.46(8)	−0.26(7)	0.53(8)	−2.00(1)	−1.20(4)	0.503(1)
a3	−3.50(3)	0.46(8)	−0.26(7)	0.53(8)	−2.00(1)	−1.20(4)	0.977(1)
a4	3.50(3)	0.46(8)	0.26(7)	0.53(8)	2.00(1)	−1.20(4)	0.743(1)
				D_2			
b1	2.45(3)	−0.30(7)	−0.27(9)	0.000	1.72(1)	−1.03(3)	−0.058(1)
b2	2.45(3)	−0.30(7)	−0.27(9)	0.000	1.72(1)	−1.03(3)	0.058(1)
b3	−2.45(3)	−0.30(7)	0.27(9)	0.000	−1.72(1)	−1.03(3)	−0.298(1)
b4	−2.45(3)	−0.30(7)	0.27(9)	0.000	−1.72(1)	−1.03(3)	−0.183(1)
a1	−3.50(3)	−0.46(8)	0.26(7)	−0.53(8)	−2.00(1)	−1.20(4)	0.263(1)
a2	3.50(3)	−0.46(8)	−0.26(7)	−0.53(8)	2.00(1)	−1.20(4)	0.497(1)
a3	3.50(3)	−0.46(8)	−0.26(7)	−0.53(8)	2.00(1)	−1.20(4)	0.023(1)
a4	−3.50(3)	−0.46(8)	0.26(7)	−0.53(8)	−2.00(1)	−1.20(4)	−0.743(1)

the strongest candidate to account for the sudden loss of ferroelectricity at the CP-LTICP transition, as the SO components S_y^1 and S_y^2 significantly increase in magnitude. The only plausible SO-based alternative is an accidental cancellation among S_y^1, S_y^2, and L_y. However, this would be an extraordinary coincidence since the corresponding SO coupling constants may not even be of the same order of magnitude, as the exchange pathways are completely different. Furthermore, this coincidence would be required for all the RMn_2O_5 compounds and all temperatures, in spite of the significant perturbations introduced by the rare-earth magnetism.[18] The origin of the residual ferroelectricity in the LTICP is, however, a different matter. The drop in E_y ($\sim$89%) is somewhat larger than the drop in P ($\sim$80%), making it plausible that the SO mechanisms may contribute significantly to the LTICP electrical polarization.

In summary, we have determined the magnetic structure of the low-temperature incommensurate phase of YMn_2O_5 from single-crystal neutron-diffraction data. By employing corepresentation analysis, we have imposed strict symmetry and physical constraints, so that all components of the electrical polarization lie along the b axis, as observed experimentally. Quantitative analysis of the magnetic structure change across the commensurate-incommensurate transition identifies exchange striction as the primary origin of ferroelectricity in this system.

APPENDIX: TABLE WITH FULLPROF PARAMETERS

See Table IV for YMn_2O_5 LTICP magnetic structure at $T=2$ K for the two domains using the FULLPROF conventions.[16]

[1] N. Hur *et al.*, Nature (London) **429**, 392 (2004).
[2] T. Kimura *et al.*, Nature (London) **426**, 55 (2003).
[3] M. Kenzelmann *et al.*, Phys. Rev. Lett. **95**, 087206 (2005).
[4] G. Lawes *et al.*, Phys. Rev. Lett. **93**, 247201 (2004).
[5] M. Mostovoy, Phys. Rev. Lett. **96**, 067601 (2006).
[6] C. Jia *et al.*, Phys. Rev. B **76**, 144424 (2007).
[7] D. Higashiyama *et al.*, Phys. Rev. B **72**, 064421 (2005).
[8] L. C. Chapon *et al.*, Phys. Rev. Lett. **93**, 177402 (2004).
[9] J. J. Betouras *et al.*, Phys. Rev. Lett. **98**, 257602 (2007).
[10] Y. Bodenthin *et al.*, Phys. Rev. Lett. **100**, 027201 (2008).
[11] C. Vecchini *et al.*, Phys. Rev. B **77**, 134434 (2008).
[12] H. Kimura *et al.*, J. Phys. Soc. Jpn. **76**, 074706 (2007).
[13] P. G. Radaelli and L. C. Chapon, J. Phys.: Condens. Matter **20**, 434213 (2008).
[14] L. C. Chapon *et al.*, Phys. Rev. Lett. **96**, 097601 (2006).
[15] J.-H. Kim *et al.*, Phys. Rev. B **78**, 245115 (2008).
[16] J. Rodríguez-Carvajal, Physica B **192**, 55 (1993).
[17] P. G. Radaelli and L. C. Chapon, Phys. Rev. B **76**, 054428 (2007).
[18] G. Beutier *et al.*, Phys. Rev. B **77**, 172408 (2008).